Pageoph,
Vol. 113 (1975)

Birkhäuser Verlag, Basel

The Short-Term Influence of Various Concentrations of Atmospheric Carbon Dioxide on the Temperature Profile in the Boundary Layer

By WILFORD G. ZDUNKOWSKI, JAN PAEGLE and FALKO K. FYE[1])

Summary – A radiative-conductive model is constructed to study short-term effects of various carbon dioxide concentrations on the atmospheric boundary layer for different seasons. The distribution of the exchange coefficient is modeled with the aid of the KEYPS formula. Infrared radiation calculations are carried out by means of the emissivity method and by assuming that water vapor and carbon dioxide are the only radiatively active gases. Global radiation is computed by specification of Linke's turbidity factor.

It is found that doubling the carbon dioxide concentration increases the temperature near the ground by approximately one-half of one degree if clouds are absent. A sevenfold increase of the present normal carbon dioxide concentration increases the temperature near the ground by approximately one degree. Temperature profiles resulting from presently observed carbon dioxide concentration and convective cloudiness of 50 % or less are compared with those resulting from doubled carbon dioxide concentrations and the same amounts of cloud cover. Again, it is found that a doubling of carbon dioxide increases the temperature in the lower boundary layer by about one-half of one degree.

The present results are obtained on the basis of fixed temperature boundary conditions as contrasted to the study of MANABE and WETHERALD (1967). However, the conclusions are not addressed to global climate change, but to the distribution of the temperature of the air layer near the ground.

1. Introduction

One facet of the recent interest expressed in atmospheric pollution is the effect of increasing carbon dioxide concentrations on the average temperature near the earth's surface. Quantitative appraisals, however, are extremely difficult in view of the complex interactions among atmospheric parameters.

PLASS (1959, 1961) has long been a proponent of the carbon dioxide theory of climatic change. He uses a radiation model to show that increased carbon dioxide concentrations result in a temperature increase in the lower atmosphere. Secondary effects such as transfer of sensible heat, water vapor content, latent heat, and cloudiness are evaluated qualitatively. KAPLAN (1960) extends Plass's model by the inclusion of clouds and shows that Plass's results of the temperature change are largely overestimated. He concludes that carbon dioxide concentration increases of an order of magnitude would be necessary to have a noticeable effect on the climate. A short-coming of both papers is the disregard of the important carbon dioxide–water vapor spectral overlap. Therefore, KONDRATIEV and NIILISK (1960) re-examine the 15 μ water vapor–carbon

[1]) Department of Meteorology, University of Utah, Salt Lake City, Utah 84112.

dioxide band and show that the overlap strongly diminishes the effect of carbon dioxide variations on boundary layer temperatures.

MÖLLER (1963) extends previous studies by treating the carbon dioxide overlap with water vapor and the effects of clouds. He finds that the surface temperature would increase or decrease, respectively, by 1.5 Celsius degrees for doubling or halving the amount of carbon dioxide if the water vapor concentration remains constant. However, if an increase in water vapor content is permitted with rising temperature, self-amplification occurs which results in almost arbitrary temperature changes. This prompted MANABE and WETHERALD (1967) to extend then available calculations by utilizing a radiation model and by applying a convective adjustment by a procedure where the temperature lapse rate in the troposphere cannot exceed 6.5 degrees per kilometer. For doubling of the carbon dioxide from 300 to 600 ppm and fixed relative humidity, they find a temperature increase of the earth's surface ranging from 2.92 to 2.36°C as sky conditions change from clear to average cloudiness.

Various authors such as NEWELL and DOPPLICK (1970), NEWELL *et al.* (1972), evaluate the effects of carbon dioxide changes using increasingly sophisticated radiation models. Due to the many interactions of energy transfer in the atmosphere, however, it is extremely difficult to extract reliable quantitative conclusions as to the effect on climate.

In a recent paper, RASOOL and SCHNEIDER (1971) suggest, on the basis of a simple radiation model, that carbon dioxide effects viewed from the pollution standpoint may not be as critical as aerosol effects. ZDUNKOWSKI and MCQUAGE (1972), using a fairly elaborate radiative-conductive model, also show that the effects of haze have important short-term implications. The effect of increased carbon dioxide, however, is not treated in their paper.

The present model definitely does not seek quantitative conclusions as to the effect of carbon dioxide on climatic changes. The objective of this paper is to determine if appreciable changes in carbon dioxide content have important short-term effects on the temperature regime of the boundary layer. It is assumed that above the top boundary (4000 m) the temperature profile of the atmosphere remains fixed to the seasonal average over the period of temperature prediction. No restriction, however, is placed in any way upon the lapse rate in the boundary layer itself. The overlap effects of carbon dioxide and water vapor in the 15 μ band are taken into account. The effect of cloudiness, at times, is estimated, and the soil layer, not previously considered, is included in the analysis.

2. *Mathematical analysis*

2.1. *List of symbols*

A list of the more important symbols is given first.

T, θ, T_s temperature and potential temperature of the air, temperature of the soil

t time

z, z_0 height and roughness height
p pressure
ρ, C_p density and specific heat at constant pressure for air
ρ_s, C_s density and specific heat for soil
F_1, F_2, F_n radiative upward, downward, and net flux
K, K_s exchange coefficients of heat for air and soil
B Stefan–Boltzmann function
u optical pathlength of atmospheric absorber
ε, τ, A, r emissivity, transmissivity, absorptivity, reflectivity
k absorption coefficient
$\rho_{CO_2}, \alpha_{CO_2}$ density and specific volume of carbon dioxide
ϑ_0 solar zenith angle
J_0 solar constant
g gravitational acceleration
N cloudiness in tenths
Γ scale factor on cloud height
G_r global radiation

2.2. Basic equations

The equations used to forecast the vertical temperature distribution in the soil and the atmosphere, with minor modification in notation, are taken from ZDUNKOWSKI and MCQUAGE (1972).

$$\frac{\partial T_s}{\partial t} = \frac{\partial}{\partial z}\left(K_s \frac{\partial T_s}{\partial z}\right), \qquad z < 0,\ t > 0 \tag{2.1}$$

$$\frac{\partial \theta}{\partial t} = \frac{\partial}{\partial z}\left(K \frac{\partial \theta}{\partial z}\right) - \frac{1}{\rho C_p}\frac{\partial F_n}{\partial z}\left(\frac{1000}{p}\right)^{0.286}, \qquad z, t > 0. \tag{2.2}$$

The effect of solar heating by atmospheric water vapor is included in the divergence of the net flux. As stated by MÖLLER (1963), carbon dioxide absorption of the sun's energy can be safely omitted. In case of cloudiness weighted means, using cloudiness as weighting factor, are required to calculate radiative temperature changes. Latent heat effects are assumed to be absent. The impact of this simplification is uncertain and any speculative discussion would not clarify the matter.

The required boundary condition for the air–soil interface and conditions at infinity are given by

$$G_r - F_{n,\,\mathrm{LW}} + \rho C_p K \frac{\partial \theta}{\partial z} - \rho_s C_s K_s \frac{\partial T_s}{\partial z} = 0, \qquad z = 0,\ t > 0$$

$$\left.\begin{aligned} T_{\mathrm{air}} &= T_s, & z &= 0 \\ \theta &= \mathrm{const}, & z &= \infty \\ T_s &= \mathrm{const}, & z &= -\infty \end{aligned}\right\} t \geqslant 0 \tag{2.3}$$

$F_{n,\,\mathrm{LW}}$ stands for the long wave net flux under cloudy conditions. If the superscript 'c' represents the clear sky, then, according to PHILIPPS (1962),

$$F_{n,\,\mathrm{LW}} = F^{c}_{n,\,\mathrm{LW}}(1 - N + N\Gamma). \tag{2.4}$$

Cloud cover affecting global radiation, G_r, is discussed in Section 2.4. Next, the component parts of these equations are examined in some detail.

2.3. Net flux of long-wave radiation

The long-wave fluxes required by the flux divergence term and interface equation are computed utilizing the emissivity method of RODGERS (1967). This approach is theoretically well founded and permits the treatment of the water vapor–carbon dioxide overlap in the 15 μ spectral region. Water vapor emissivities are usually taken from Rodgers while carbon dioxide absorption data is taken from another source as described later. The emissivities and transmissivities are expressed in terms of pressure corrected absorber amounts and are justifiably taken as independent of temperature for water vapor. In the case of carbon dioxide, temperature dependency of these quantities must be considered. The effect of ozone is omitted since it is very small.

With these assumptions the total upward flux at the reference level z_R is given by

$$\begin{aligned} F_1(z_R) = {} & B(0)[1 - \varepsilon_{1,\mathrm{H_2O}}(z_R, 0)] + \int_{z_R}^{0} B(z') \frac{d\varepsilon_{1,\mathrm{H_2O}}(z, z')\,dz'}{dz'} \\ & + 277 \left\{ \int_{z_R}^{0} B_{667}(z') \frac{d}{dz'} [\varepsilon_{\mathrm{CO_2}}(z, z')\tau_{\mathrm{H_2O}}(z, z')]\,dz' \right. \\ & \left. - B_{667}(0)\,\varepsilon_{\mathrm{CO_2}}(z_R, 0)\,\tau_{\mathrm{H_2O}}(z_R, 0) \right\}. \end{aligned} \tag{2.5}$$

$B(0)$ stands for the upward flux at the earth's surface. The third term on the right-hand side of (2.5) accounts for the water vapor–carbon dioxide overlap. The factor 277 refers to the spectral width of the overlap region in units of $\mathrm{cm^{-1}}$ and 667 $\mathrm{cm^{-1}}$ represents the band center. The corresponding expression for the downward flux is

$$F_2(z_R) = \int_{z_R}^{\infty} B(z') \frac{d\varepsilon_{2,\mathrm{H_2O}}(z, z')}{dz'} dz' + 277 \int_{z_R}^{\infty} B_{667}(z') \frac{d}{dz'} [\varepsilon_{\mathrm{CO_2}}(z, z')\tau_{\mathrm{H_2O}}(z, z')]\,dz'. \tag{2.6}$$

Note that the overlap region given by Rodgers is taken as 200 $\mathrm{cm^{-1}}$, but is expanded here so as to include the entire carbon dioxide band (528.5–805.5 $\mathrm{cm^{-1}}$).

Upward (ε_1) and downward (ε_2) water vapor emissivities required a small amount of smoothing near the pathlength of 10^{-3} gm/cm^2.

The water vapor transmission for the overlap calculations is derived from the absorption data of YAMAMOTO and ONISHI (1949) and is used here in the form given by KONDRATIEV and NIILISK (1960), i.e.

$$\tau_{H_2O} = \frac{1}{B_{667}\,\Delta\nu} \sum_i B_i\, e^{-k_i \mu}\, \Delta\nu_i. \tag{2.7}$$

The band width, $\Delta\nu$, as before, extends from 528.5 to 805.5 cm^{-1}. Test calculations show that the temperature variation of τ_{H_2O} is entirely negligible for the atmospheric range.

A selection of suitable carbon dioxide absorption data presents a difficult problem. The agreement of absorption curves as given by various authors is far from satisfactory. These deviations are especially pronounced in the region of large and small absorbing masses. The problem is compounded by the lack of consistency with respect to size of the spectral interval and temperature used by the authors.

The carbon dioxide absorption curve selected for use here is the result of theoretical calculations by YAMAMOTO and SASAMORI (1958) and applies to the spectral region from 528.5 to 805.5 cm^{-1} and a temperature of 300 K. This curve is approximated by KONDRATIEV and NIILISK (1960) by the relation

$$A = 10^{(a+bu^c)^d} \tag{2.8}$$

where a, b, c, and d are empirical coefficients provided in the original paper. Temperature dependence of carbon dioxide emission is not negligible and is accounted for in an approximate manner. To gain the desired temperature dependence, a set of tabulated emissivity curves from SASAMORI (1958) is employed and is shown in Fig. 1 together with the adopted basic emissivity curve ($T = 300$ K).

The temperature dependence is accounted for by using an effective layer temperature to obtain the carbon dioxide emissivity (DAVIS, 1961)

$$T_e = \int Tp\, dp / \int p\, dp. \tag{2.9}$$

Conversion from beam to diffuse radiation is accomplished with the aid of the diffusivity factor, $\beta = 1.66$. This approximation is applied in all cases except for Rodgers' water vapor emissivities where the diffusivity factor is already included.

The necessary optical pathlengths for water vapor and carbon dioxide are found from

$$u_{H_2O} = \int \rho_v(z) \frac{p}{p_0}\, dz \sqrt{\frac{T_0}{T}} \left[\frac{gm}{cm^2}\right]. \tag{2.10}$$

$$u_{CO_2} = \alpha_{CO_2}(\mathrm{NTP}) \int \rho_{CO_2}(z) \left(\frac{p}{p_0}\right)^{0.8} \sqrt{\frac{T_0}{T}}\, dz [\mathrm{atm\,cm}]. \tag{2.11}$$

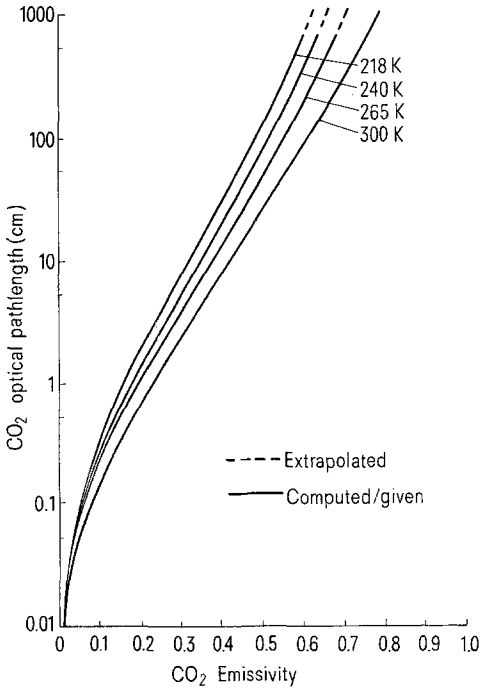

Figure 1
Comparison of emissivity curves for carbon dioxide for various temperatures

Stratospheric moisture is extrapolated from the given tropospheric value to zero at the stratopause while carbon dioxide calculations include the entire atmosphere. Details of the moisture distribution are discussed in Section 2.6. Radiation calculations are carried out using the finite difference scheme explained in the appendices. Near the reference level, however, integration is always carried out over very thin layers to account for the radiative 'near effect'.

2.4. Solar radiation

The boundary condition at the earth's interface requires a knowledge of the global radiation. An exact mathematical treatment of this quantity is possible but prohibitively expensive. Therefore, the global radiation is expressed by the semi-empirical expression of PHILIPPS (1962) which was previously used by ZDUNKOWSKI and MCQUAGE (1972). For details see either paper.

The global radiation, G_r, representing the combined effects of diffuse and direct solar radiation, is expressible in terms of Linke's turbidity factor, τ_L, and is given by

$$G_r = J_0(0.755 - 0.054\tau_L)(1 - 0.66N)\cos\nu. \tag{2.12}$$

The expression implicitly contains an average ground reflectivity of 20%. The $\cos\vartheta_0$ is found from well-known relationships of mathematical astronomy which are not repeated here. The quantity needed to determine τ_L is defined as

$$\tau_L = \frac{(\beta_R + \beta_w)}{\beta_R}. \tag{2.13}$$

Here β_R and β_w are the complex Rayleigh scattering and water vapor absorption coefficients, respectively.

According to FEUSSNER and DUBOIS (1930), β_R can be found accurately from

$$\beta_R = \ln\left(\frac{1}{0.907 m_l^{0.018}}\right) \tag{2.14}$$

where m_l is the air mass and approximately equals $\sec\vartheta_0$ for solar zenith angles ϑ_0 less than 60°. For $\vartheta_0 > 60°$, tabular corrections are applied.

The quantity β_w can be reduced to the following form using MCDONALD's (1960) absorption data

$$\beta_w = \frac{-1}{\sec\vartheta_0} \cdot [\ln(1.0 - 0.077 u'^{0.30})]. \tag{2.15}$$

The quantity u' equals $u_{H_2O} \sec\vartheta_0$.

The heating effect due to water vapor absorption of solar radiation, though small, is treated (MCDONALD, 1960) for completeness and is included in the divergence of net flux.

2.5. Formulation of the exchange coefficient

The model requires an accurate description of the exchange coefficient for the diffusion of heat to adequately predict the temperature of the boundary layer. In the interest of simplicity and economy, an exchange coefficient is used which does not require a solution of the equations of motion. A simple, yet fairly accurate form of the exchange coefficient is found by solving the so-called KEYPS formula which is based on the similarity theory. The formula, applied successfully by PILIE *et al.* (1972) and others, is given as

$$K = \frac{k' z}{\sqrt{2}} \left\{ -\gamma \frac{g}{T} \frac{\partial\theta}{\partial z} (k' z)^2 + \left[\left(\gamma \frac{g}{T} \frac{\partial\theta}{\partial z} (k' z)^2 \right)^2 + 4u^{*4} \right]^{1/2} \right\}^{1/2}. \tag{2.16}$$

Here k' is von Karman's constant, $\gamma = 14$ is an empirical stability number, and friction velocity u^* is chosen as 0.30 which, for neutral conditions, corresponds to a geostrophic wind of approximately 10 m sec^{-1} and a roughness height of 1 cm.

Inspection of (2.16) shows that the exchange coefficient is zero at the surface which

is an unrealistic situation in that it would not permit heat flow through the interface. For this reason, a small residual value of the exchange coefficient is added. It is assumed that the exchange coefficient at the soil interface during the nighttime is five times as large as the molecular diffusion coefficient. During unstable conditions near the surface, the value of the exchange coefficient at the interface is assumed to be slightly less than the computed value at the roughness height.

Formula (2.16) is strictly valid only for the air layer near the ground, but is applied here to the entire boundary layer. For this reason, in the presence of a nearly dry adiabatic boundary layer, the exchange coefficient increases with height to unreasonably large values at the top of the boundary layer. To limit the value of the exchange coefficient it is assumed that it reaches a maximum at some elevation and decreases at higher levels. In case of nearly dry adiabatic conditions, the height of the maximum is arbitrarily chosen such as to limit the maximum value of the exchange coefficient. Variation of this height from 500 m to 1000 m has significant effect on the profile of K, but not in the evolution of the temperature profile near the surface. If the boundary layer is not neutrally stratified, (2.16) provides a maximum value and the height at which the maximum occurs. Above this height of the maximum exchange coefficient, K is decreased according to an extrapolation technique which decreases the exchange coefficient with height in a nonlinear fashion to avoid large values in the upper portion of the boundary layer. The extrapolation formulation is stated as

$$K_j = K_{\max}/(1 + 10^{-6}(z_j - z(K_{\max}))^2). \tag{2.17}$$

Some numerical details for K are given later on.

2.6. Determination of initial and boundary conditions

Three seasonal cases for spring, summer, and winter are considered. Each requires an initial distribution of temperature, pressure, and moisture. From this data, the water vapor and carbon dioxide optical depths are obtained. The exchange coefficient is then calculated directly from the initial temperature profile. Predictions are carried out for six days when all cases display a periodicity of 24 hours and transient effects are no longer evident.

The U.S. Standard Atmosphere (1962) is used for the springtime situation and supplement atmospheres as given by VALLEY (1965) are applied for the July and January cases. Latitude is always assumed to be 45 degrees north. Initial moisture profiles are also given by Valley in terms of relative humidity. Values are reduced by a few percent near the surface, if necessary, to preclude fog formation. Effects of moisture enter the calculations only through the optical pathlength of water vapor. Time changes in absolute humidity in the absence of sources or sinks are assumed to be sufficiently slow so that they may be neglected for the duration of the prediction period. This is a more satisfactory assumption than that of constant relative humidity near the ground for the present model which includes diurnal variations.

The case of a dry cloudless springtime atmosphere is considered. To prevent the occurrence of convective clouds, a height constant tropospheric relative humidity of 25% is assumed which is decreased to zero at 20 km. Such a moisture distribution is typical of semi-arid regions. A second springtime tropospheric model (VALLEY, 1965) assumes a boundary layer relative humidity of 60% which decreases with height to near 20% at the tropopause and then to zero at 20 km. The January moisture data consists of a 65% relative humidity near the surface, decreasing to 30% at the tropopause and zero at 20 km. A nearly identical relative humidity distribution is adopted for the July model.

Soil temperature profiles are obtained from GEIGER (1966) and are selected to coincide with the atmospheric profile. The soil is assumed to be sandy clay ($\rho_s = 1.78$ gm cm^{-3}, $C_s = 0.33$ cal gm^{-1} K^{-1}, $K_s = 0.0037$ cm^2 sec^{-1} (JOHNSON, 1954)).

Numerical experimentation shows that the soil temperature remains unaffected for the duration of the prediction period below a depth of one meter. A constant soil temperature for each season at one-meter depth is taken as the lower boundary condition.

Since the atmosphere above the boundary layer shows no diurnal temperature variation, it is assumed that potential temperature remains constant in time above this height and has a fixed distribution regardless of the carbon dioxide concentration. The initially assumed potential temperatures for each season at the top of the prediction layer are considered as the boundary values for the diffusion analysis. Radiative flux computations, however, cannot be discontinued at the top of such a layer and therefore include the entire atmosphere. To have a consistent model, however, radiative temperature changes above the upper boundary, assumed to be fixed at a height of 4 km, are disregarded. Such effects should be largely counter-balanced by large-scale tropospheric motion as empirically evidenced by the small average temperature changes within a season.

The constraint of constant temperature at the upper boundary and one meter below the soil surface may have some quantitative influence on the results. For the soil case of constant conductivity, the penetration depth would be $\sqrt{K_s \times 6 \text{ days}}$ (about 40 cm) for a six-day forecast. It is therefore unlikely that the assumption of constant temperature at a depth of one meter below the surface would have any important quantitative effect on the results in the atmosphere. Various experiments were made varying the conditions at the top of the planetary boundary layer. The formulation of K described previously is such that the results in most of the planetary boundary layer are insensitive to the upper boundary condition.

Numerical techniques used in this study are discussed in the appendices.

3. *Discussion of results*

From physical principles it is clear that the adopted initial temperature distribution of the boundary layer is not necessarily in equilibrium with the radiation regime existing for a particular time of the year. Consider, for example, the initial temperature

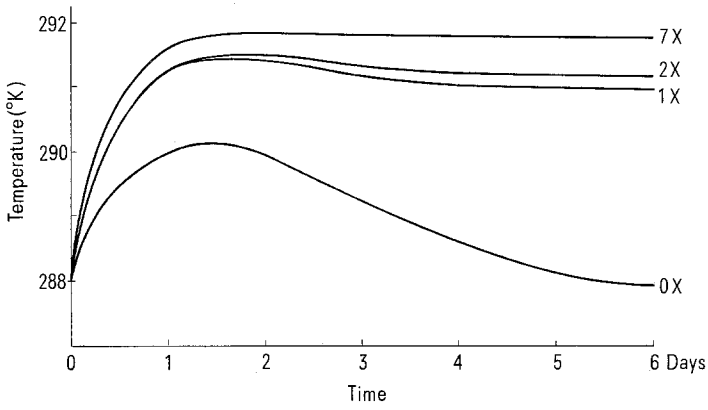

Figure 2
Temperature convergence of the method at a height of 1.5 m for time of sunset during springtime and for varying concentrations of carbon dioxide. × means times normal CO_2 concentration

profile of the cloudless U.S. Standard Atmosphere at the time of the vernal equinox. The physical system readjusts itself to a diurnal temperature oscillation which reproduces itself from day to day after transient modes have damped. This is demonstrated

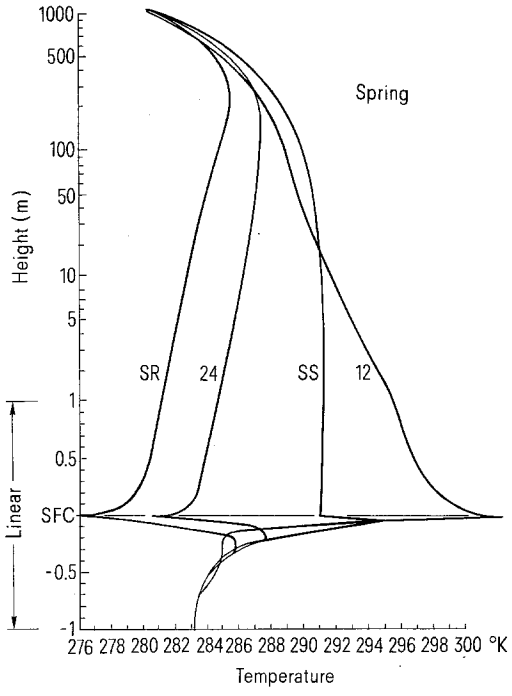

Figure 3
Distribution of air and soil temperature for characteristic times of the day at the vernal equinox, no clouds, and a normal carbon dioxide concentration. SR—sunrise, SS—sunset, 12—noon, 24—midnight of sixth day

in Fig. 2 for the time of sunset. The slowest adjustment occurs for the fictitious case that there is no carbon dioxide in the atmosphere, while it proceeds more rapidly with increased carbon dioxide. The symbol × indicates the number of times of the normal (presently observed) carbon dioxide concentration. At the surface of the earth, the adjustment requires a similar period of time, but proceeds more rapidly with increasing height. Similar conditions exist for the other initialization models.

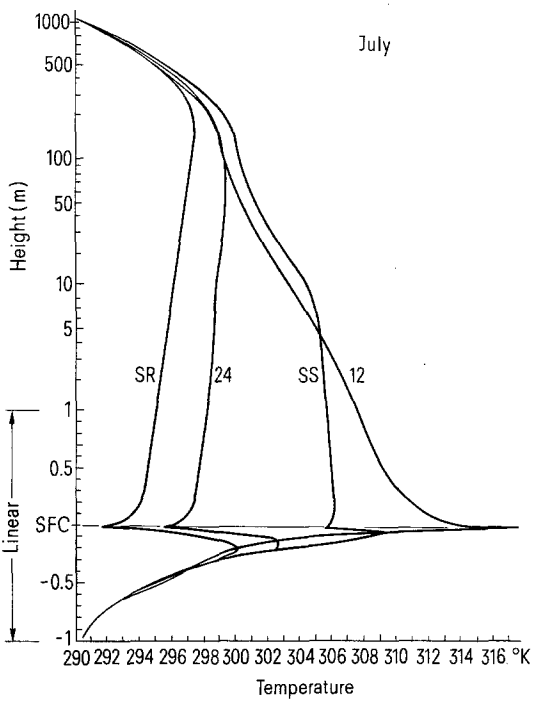

Figure 4
Distribution of air and soil temperature for characteristic times of the day in late July with three-tenths of convective cloudiness near the top of the boundary layer and a normal carbon dioxide concentration

With the model in final state, it is possible to examine the validity of the predicted temperature profiles within the boundary layer. Figures 3, 4, and 5 illustrate the diurnal temperature variation for the normal (300 ppm), presently observed, carbon dioxide concentration in the lower atmosphere and in the soil for the three seasonal cases considered. Inspection shows that the temperature distribution within the lower atmosphere and within the soil shows a reasonable behavior and compares favorably with numerous low-level observed temperature profiles given by GEIGER (1966). However, Geiger's data is insufficient to make specific comparisons. The springtime situation refers to the vernal equinox and appears to give unseasonably high surface temperatures. The reason is that the calculations refer to a cloudless and aerosol-free atmosphere and a soil moisture of only 15%. The soil moisture content in this context enters only

through the soil constants through the diffusion equation and interface condition. In true situations, however, the soil might be partly covered by snow and considerable cloudiness might be present. Further inspection shows that realistic physical features such as nocturnal temperature inversions and superadiabatic lapse rates at noontime are faithfully reproduced in all situations.

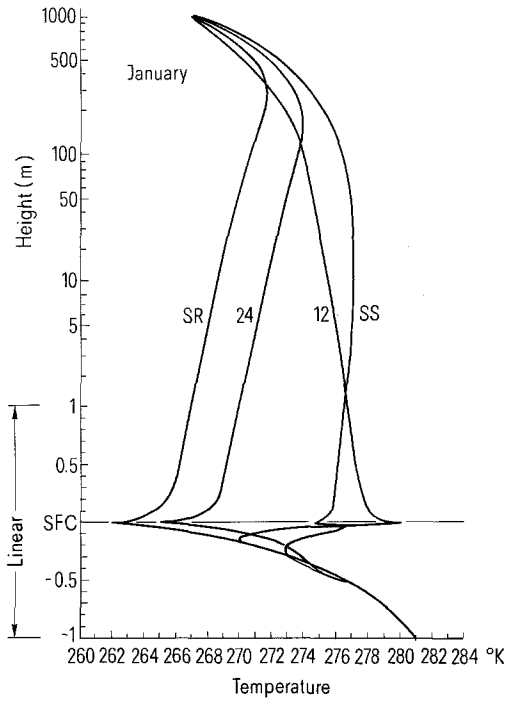

Figure 5
Distribution of air and soil temperature for characteristic times of the day in mid-January with no clouds and a normal carbon dioxide concentration

It is of interest to consider the seasonal distribution of the exchange coefficients (Fig. 6). Observed realistic features are reproduced by the model. The maximum and minimum values are found at the time of maximum and minimum surface temperature, respectively. The height of the maximum values of the exchange coefficient increase from sunrise to the time of maximum temperature. In addition, the low level increase is nearly linear. Generally larger values are observed in summer than in winter. Further details on the exchange coefficient are given in Appendix C.

Of considerable interest are the effects of atmospheric flux divergence upon the formation of the temperature profile. At the time of maximum temperature with superadiabatic lapse rates near the ground, instantaneous radiative cooling of the air directly overlying the ground is occasionally as large as 35 degrees per hour. Radiative heating of the air layer at the ground at the time of the strongest ground inversion is of the order

of 10 degrees per hour. These results are in agreement with similar radiative temperature change calculations by MÖLLER (1955) and ZDUNKOWSKI and JOHNSON (1965) although their computational methods are entirely different and are based on different absorption data. The validity of the present carbon dioxide calculations is verified against similar results obtained by PLASS (1959, 1961), KONDRATIEV and NIILISK (1960), and MANABE and MÖLLER (1961). A specific direct comparison may, however, be inappropriate

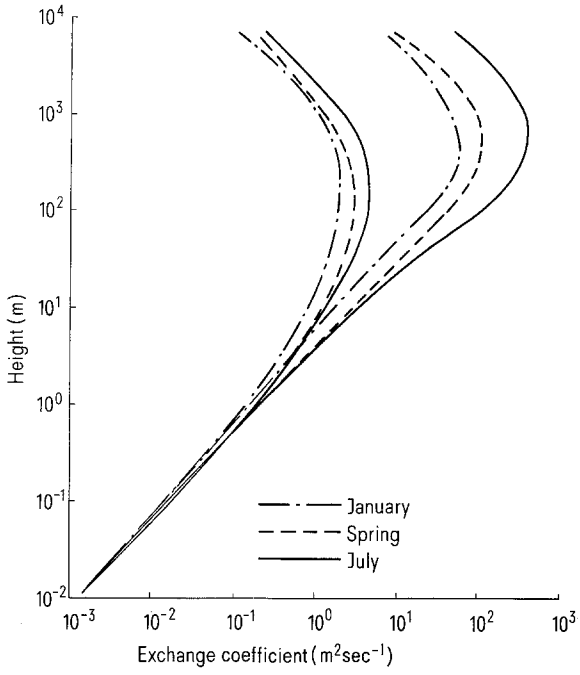

Figure 6
Seasonal distribution of the exchange coefficient at the times of maximum and minimum temperature. Larger values refer to daytime

because of differences in various model parameters such as temperature, moisture, absorption and spectral data. The much smaller predicted actual temperature changes lead to the conclusion that the large radiative temperature changes near the ground are strongly counterbalanced by exchange processes. This confirms MÖLLER's (1955) conclusion that radiative flux divergence in nonpolluted air has only minor influence on the temperature profile. Indeed, assuming that the radiative flux divergence is completely absent during the springtime and summer day, results in nearly unaltered temperature profiles of the atmosphere and soil. Nevertheless, all calculations include the effect of radiative flux divergence.

Consider next the effects of variable carbon dioxide concentrations as shown in Figs. 7, 8, 9, and 10. Each figure considers the four different cases of interest. The first fictitious case assumes that the air does not contain any carbon dioxide. The second

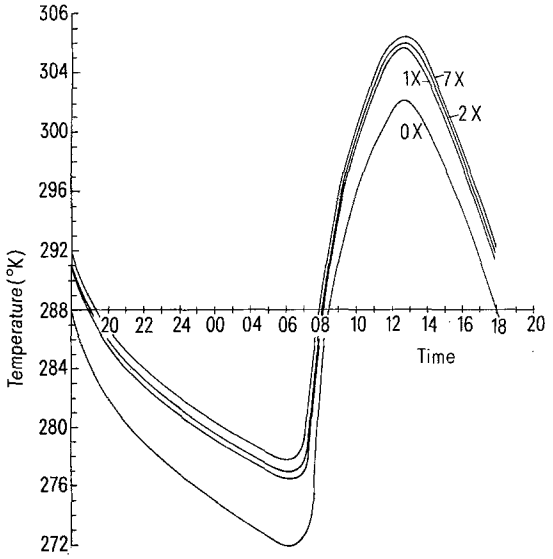

Figure 7
Diurnal temperature variation for various carbon dioxide concentration at the surface of the earth and at the time of the vernal equinox. The × indicates times normal concentration. No clouds

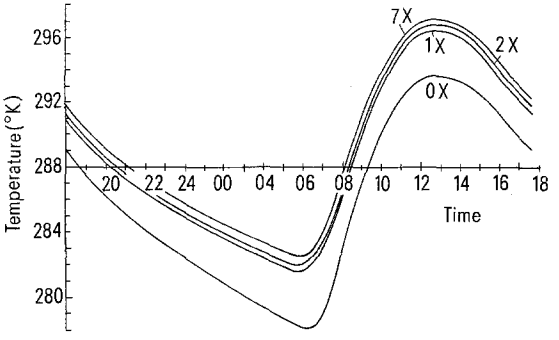

Figure 8
Diurnal temperature variation for various carbon dioxide concentrations at a height of 1.5 m and at the time of the vernal equinox. The × indicates times normal concentration. No clouds

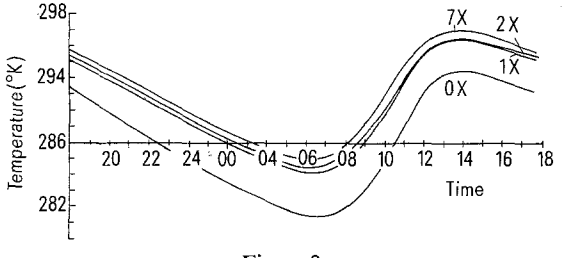

Figure 9
Diurnal temperature variation for various carbon dioxide concentrations at a height of 30 m and at the time of the vernal equinox. The × indicates times normal concentration. No clouds

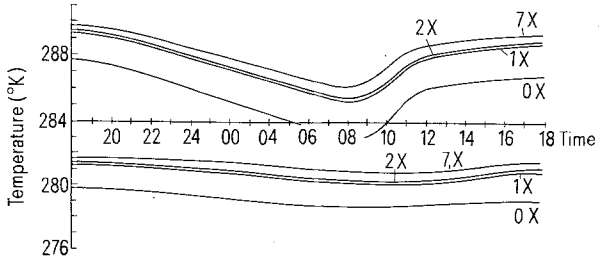

Figure 10
Diurnal temperature variation for various carbon dioxide concentrations at heights of 220 m (upper) and 1050 m (lower) at the time of the vernal equinox. The × indicates times normal concentration. No clouds

case considers the normal, presently observed concentration, while Case 3 considers twice the normal concentration to be expected after many decades. Seven times the normal concentration, as considered in Case 4, probably represents a physical upper bound.

The most conspicuous result is the large temperature decrease from the normal carbon dioxide concentration to the physically unrealistic situation that the concentration is zero. All levels reveal this anomaly, but it is most pronounced at the surface of the earth. Increasing carbon dioxide from the normal, however, alters the temperature only slightly. The effect of doubling the CO_2 concentration to twice current values raises the surface temperature by 0.30 to 0.36°C with an average of 0.33°C during the sixth day of integration for cloudless, moist spring conditions. For dry, but otherwise identical conditions, this rise is a tenth of a degree larger, and for July conditions, slightly higher yet. Thus it seems that the effect of doubling CO_2 concentrations above currently observed values increases temperature in this model by almost 0.5°C. For seven times normal concentrations, the average temperature increase is about 1°C with slight seasonal variability. All cases produce temperature changes which are generally uniform in height and time in the lower section of the model atmosphere.

To show that the effect of carbon dioxide is consistent for different seasons, cases for January and July are considered and shown by Figs. 11 and 12, respectively. Results

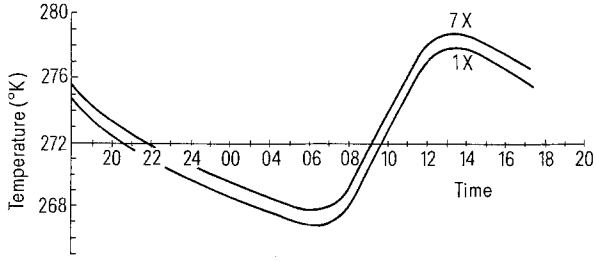

Figure 11
Diurnal temperature variation for two carbon dioxide concentrations at a height of 1.5 m in mid-January with no clouds present. The × indicates times normal concentration

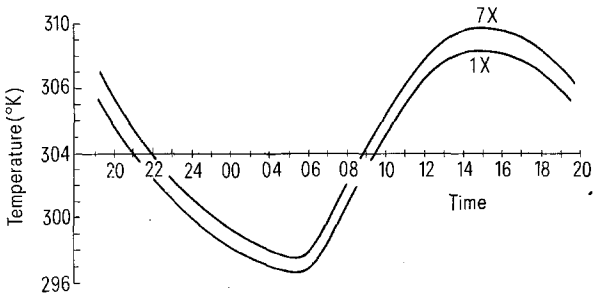

Figure 12
Diurnal temperature variation for two carbon dioxide concentrations at a height of 1.5 m in late July with three-tenths of clouds present. The × indicates times normal concentration

agree well with the springtime studies. With the aid of the thermodynamic chart, it is estimated that in the July case, convective clouds form at a height of 2.5 km at 10 a.m. and begin dissipation at 3 p.m. The estimated average cloud cover, N, equals 0.3. In the present simple model, cloud cover and height effect only the radiative calculations. Even with the presence of clouds, the effects of increased carbon dioxide are in close agreement with the springtime cases where no clouds are present. One degree of temperature rise is predicted, as before, in the lower kilometer.

Figure 13 compares the effect of one-tenth of cloudiness, cloud height 2.5 km, in springtime for a normal carbon dioxide concentration with the case of a cloudless sky and twice the normal content of carbon dioxide. Also shown for comparison is the case of normal carbon dioxide with no clouds. All cases have identical moisture profiles

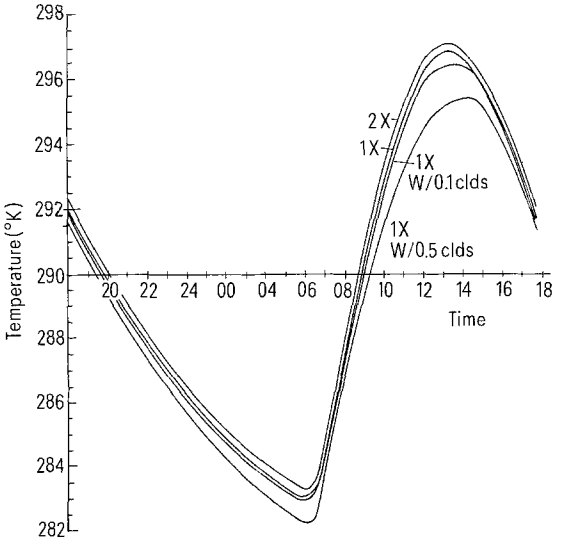

Figure 13
Diurnal temperature variation at the vernal equinox for various carbon dioxide concentrations and various amounts of cloud cover. All cases contain a moist atmosphere

with a relative humidity of 60% in the boundary layer decreasing to 20% at the tropopause and to zero near 20 km. An additional case of 50% cloudiness and normal carbon dioxide concentration shows an average cooling in excess of one-half of one degree. It is seen, that while a carbon dioxide content of twice the normal concentration accounts for a small temperature increase, the addition of one-tenth of cloudiness to an atmosphere of normal carbon dioxide content accounts for a decrease of a similar magnitude.

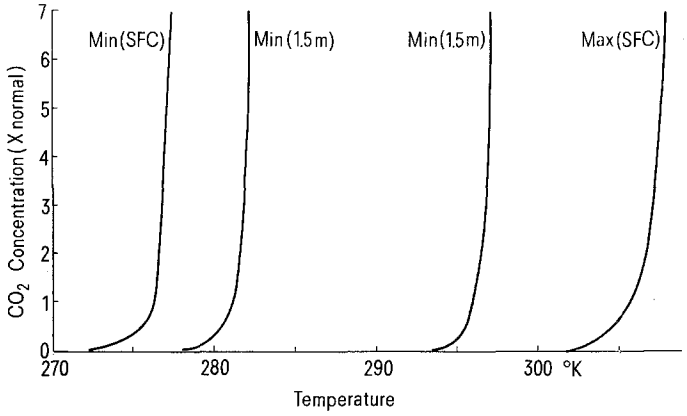

Figure 14
Effect of variable carbon dioxide concentrations on maximum and minimum temperature at the surface and at 1.5 m at the time of the vernal equinox and a cloudless sky

The effects of varied carbon dioxide concentrations on the air layer near the earth's surface are summarized in Fig. 14 for the springtime case in the absence of cloudiness. The greatest temperature variation is found as the carbon dioxide concentration is varied from the fictitious case of no carbon dioxide to the case of a normal, presently observed carbon dioxide concentration. Additional increases account for only small temperature rises even when seven times the normal concentration is considered.

4. Conclusion

This study indicates that on a short-term basis, expected variations of the carbon dioxide concentration do not have a pronounced effect on the temperature distribution of the boundary layer. Doubling the carbon dioxide concentration causes an overall temperature increase of the air near the ground by approximately one-half of one degree if clouds are absent. For twice the normal concentration and cloud cover of less than 50%, the same temperature increase is observed. If the carbon dioxide concentration is increased to seven times the presently considered normal value, the temperature near the ground is increased by one degree. In the fictitious clear sky case that the air does not contain any carbon dioxide, the temperature in the lower portion of the boundary layer decreases by approximately two degrees as compared to the normal carbon dioxide concentration.

Consider the springtime situation with a moist boundary layer, one-tenth of convective cloudiness and normal carbon dioxide concentration. This amount of cloudiness decreases the temperature near the ground by about one-half of one degree while doubling the carbon dioxide concentration with no clouds increases the temperature by a similar amount. In all situations it is found that the basic observed features of the lower atmosphere, such as nocturnal temperature inversions and mid-day superadiabatic lapse rates, are faithfully reproduced.

The temperature rises due to increased carbon dioxide concentrations which are observed here are smaller than results predicted by other investigators whose calculations are usually based on static radiation models. MANABE and WETHERALD (1967), utilizing the concept of convective adjustment, report temperature rises near the surface of approximately 2°C (average value for constant absolute and relative humidity, with and without cloud cover) with a doubling of the carbon dioxide content of the atmosphere. It is realized that their thermal equilibrium prediction model addresses the general circulation scale of climatic change. However, their crude resolution of the B.L. and total neglect of the important sub-soil influences severely restrict the accuracy of their model of the air layer near the surface. Particularly, the convective adjustment to 6.5°C/km (which is close to the saturation adiabat for warm temperatures) is unrealistic within the usually unsaturated lower several hundreds of meters.

Finally, it may be in order to speculate why the present temperature increase at the surface of the earth is so much less than that obtained by MANABE and WETHERALD (1967). The most important differences in the models relate to the presence of a soil layer, treatment of upper tropospheric and stratospheric influences, of mixing processes and of horizontal variability. The temperature distribution of the air layer near the ground is most profoundly influenced by the presence of the earth's surface. Any unnatural constraint, such as a constant temperature lapse rate, or unreasonable mixing assumptions could very easily dominate low level temperature profiles.

Possibly the weakest point of the present analysis is that the temperature distribution of the air above the boundary layer is assumed to be unaffected by an increase in carbon dioxide concentrations. Such increase undoubtedly changes the temperature distribution of higher layers of the atmosphere and thus causes changes in the radiative heat budget. However, the effect of ± 2 degree temperature change of the upper boundary on the surface temperature due to eddy mixing is of very little consequence on this time scale. Further investigation on whether convective adjustment or maintenance of a constant temperature at the top boundary has greater artificial impact is now being conducted.

REFERENCES

DAVIS, P. A. (1961), A Re-examination of the Heat Budget of the Troposphere and Lower Stratosphere. Sci. Rpt. No. 3, AF 19(604)-6146, New York University, p. 18.

FEUSSNER, K., and DUBOIS, P. (1930), *Trübungsfaktor, precipitable water, Staub.*, Gerlands Beitr. Geophys. *27*, 132–175.

GEIGER, R., *The Climate Near the Ground* (Harvard Univ. Press, Cambridge, Mass. 1966), Chap. 2.
JOHNSON, J. C., *Physical Meteorology* (Tech. Press of M.I.T. and John Wiley and Son, New York 1954), p. 156.
KAPLAN, L. D. (1960), *The influence of carbon dioxide variations on the atmospheric heat balance*, Tellus *12*, 204–208.
KONDRATIEV, K. Y., and NIILISK, H. I. (1960), *On the question of carbon dioxide heat radiation in the atmosphere*, Geofis. Pura. E. Applicata. *46*, 216–230.
MANABE, S., and MÖLLER, F. (1961), *On the radiative equilibrium and heat balance of the atmosphere*, Mon. Wea. Rev. *89*, 503–532.
MANABE, S., and WETHERALD, R. T. (1967), *Thermal equilibrium of the atmosphere with a given distribution of relative humidity*, J. Atmos. Sci. *24*, 241–259.
MCDONALD, J. E. (1960), *Direct absorption of solar radiation by atmospheric water vapor*, J. Meteor. *17*, 319–328.
MÖLLER, F. (1955), *Strahlungsvorgänge in Bodennähe*, Z. Meteor. *9*, 47–55.
MÖLLER, F. (1963), *On the influence of changes in the CO_2 concentration in air on the radiation balance of earth's surface and on the climate*, J. Geophys. Res. *68*, 3877–3885.
NEWELL, R. E., and DOPPLICK, T. G. (1970), *The effect of changing CO_2 concentration on radiative heating rates*, J. Appl. Meteor. *9*, 958–959.
NEWELL, R. E., HERMAN, G. F., DOPPLICK, T. G., and BOER, G. J. (1972), *The effect of changing CO_2 concentration on radiative heating rates: Further comments*, J. Appl. Meteor. *11*, 864–867.
PHILIPPS, H. (1962), *Zur Theorie des Tagesganges der Temperatur in der bodennahen Atmosphäre und in ihrer Unterlage*, Z. Meteorol. *16*, 5.
PILIE, R. J., EADIE, W. J., MACK, E. J., ROGERS, C. W., and KOCMOND, W. C. (1972), Project Fog Drops Part I—Investigation of Warm Fog Drops. Seventh Annual Summary Report, NASW-2126, pp. 106–109.
PLASS, G. N. (1959), *Carbon dioxide and climate*, Scientific American 201, 41–47.
PLASS, G. N. (1961), *The influence of infrared absorptive molecules on the climate*. Annals of the N.Y. Acad. of Sci. 61–71.
RASOOL, S. J., and SCHNEIDER, S. H. (1971), *Atmospheric carbon dioxide and aerosols: Effects of large increases on global climate*, Science *173*, 138–141.
RICHTMEYER, R. D., and MORTON, K. W., *Difference Methods for Initial Value Problems* (Interscience Publishers, New York, 1967), p. 176.
RODGERS, C. D. (1967), *The use of emissivity in atmospheric radiation calculations*, Quart. J. Roy. Meteor. Soc. *93*, 43–54.
SASAMORI, T. (1959), *The temperature effect on the absorption of 15 microns carbon-dioxide band*, Sci. Rep. Tohoku Univ., Ser. 5 *11*, No. 3.
VALLEY, S. A., ed. *Handbook of Geophysics and Space Environments* (McGraw Hill, New York 1965), Chaps. 2, 3.
YAMAMOTO, G., and ONISHI, G. (1949), *Absorption coefficient of water vapor in the far infrared region*, Sci. Rep. Tohoku Univ., Ser. 5 *1*, No. 1.
YAMAMOTO, G., and SASAMORI, T. (1958), *Calculation of the absorption of the 15 micron carbon-dioxide band*, Sci. Rep. Tohoku Univ., Ser. 5 *10*, No. 2.
ZDUNKOWSKI, W. G., and JOHNSON, F. C. (1965), *Infrared flux divergence calculations with newly constructed radiation tables*, J. Appl. Meteor. *4*, 371–377.
ZDUNKOWSKI, W. G., and MCQUAGE, N. D. (1972), *The effect of haze on a radiative, conductive, dynamic model profile of the lower atmosphere*, Tellus, *25*, 237–254.

Appendix A

Height transformations

Since the boundary layer variables exhibit very rapid fluctuations near the earth–air interface, and slower variations at larger distances from this interface, it is useful to

transform the height coordinate. This appendix presents transformations which retain accuracy and economy of computation in an explicit time differencing scheme.

The soil conduction equation is

$$\frac{\partial T_s}{\partial t} = K_s \frac{\partial^2 T_s}{\partial z^2}, \qquad z < 0. \tag{A.1}$$

Defining

$$\xi = \sqrt{-z/L}, \tag{A.2}$$

where L is a positive length, transforms (A.1) to

$$\frac{\partial T_s}{\partial t} = \frac{K_s}{4L^2}\left[-\frac{\partial^2 T}{\partial \xi^2}\frac{L}{z} - \frac{\partial T}{\partial \xi}\left(-\frac{z}{L}\right)^{-3/2}\right]. \tag{A.3}$$

In the atmosphere the turbulent mixing of potential temperature is modeled by

$$\frac{\partial \theta}{\partial t} = \frac{\partial}{\partial z}\left(K\frac{\partial \theta}{\partial z}\right). \tag{A.4}$$

Using the transformed height coordinate

$$\xi = L \ln\left(\frac{z}{z_1}\right) \tag{A.5}$$

(A.4) becomes:

$$\frac{\partial \theta}{\partial t} = \frac{\partial K}{\partial \xi}\frac{\partial \theta}{\partial \xi}\left(\frac{L}{z}\right)^2 + K\left[\frac{\partial^2 \theta}{\partial \xi^2}\left(\frac{L}{z}\right)^2 - \frac{\partial \theta}{\partial \xi}\frac{L}{z^2}\right]. \tag{A.6}$$

In the lowest few meters of the atmosphere, the exchange coefficient is practically a linear function of z (see Fig. 6). When K is linearly proportional to z it is easily shown that (A.6) simplifies to

$$\frac{\partial \theta}{\partial t} = K\frac{\partial^2 \theta}{\partial \xi^2}\left(\frac{L}{z}\right)^2. \tag{A.7}$$

While K is not precisely linear in z, the error of this approximation at grid points below 10 m appeared to be insignificant to test computations. Use of (A.7) in the lowest few meters permits much larger time steps than can be used in (A.6) in any explicit time differencing scheme.

The fully nonlinear height variation of K must be retained above the lowest few meters, but the transformation (A.5) still proves useful in the lowest 200 m. At height levels between 10 and 220 m equation (A.6) is used in complete form. Above 220 m equation (A.4) is used with equal increments in z.

Variations of the parameters L, $\Delta\xi$ and z_1 and varying the height of the layer to which the transformation is applied provides great flexibility in the resulting height coordinate system. The following selection of parameters is made in this investigation: L (soil) = 0.5 cm, L (air) = 1.0 cm, $\Delta\xi = 1.0$, $z_1 = 1.0$ cm, and the maximum height to which the transformation is applied is 220 m. The resulting height coordinates of the grid points are: –0.98, –0.85, –0.72, –0.60, –0.5, –0.4, –0.32, –0.25, –0.18, –0.13, –0.08, –0.05, –0.02, –0.005, 0.0, 0.01, 0.027, 0.074, 0.2, 0.55, 1.48, 4.03, 10.97, 29.8, 81.0, 220.3, 359.5, ..., 3701.1, 3840.3 m.

Appendix B

Finite difference approximations

Approximations with second-order accuracy in Δt, $\Delta\xi$, and Δz are used in all forecast equations. The diffusion terms are modeled using the DuFort–Frankel scheme (see RICHTMEYER and MORTON, 1967), and the time differencing is explicit throughout. The finite difference approximations for the various layers are as follows:

Soil:

$$\frac{T_j^{n+1} - T_j^{n-1}}{2\Delta t} = -\frac{K_s}{4L^2}\left(\frac{L}{z_j}\right)\left[\frac{T_{j+1}^n + T_{j-1}^n - T_j^{n+1} - T_j^{n-1}}{(\Delta\xi)^2}\right] - \frac{K_s}{4L^2}\left(-\frac{z_j}{L}\right)^{-3/2}\left[\frac{T_{j+1}^n - T_{j-1}^n}{2\Delta\xi}\right]. \tag{B.1}$$

Heat balance, interface equation:

$$G_r - F_{h,\mathrm{LW}} + C_p \rho_0 K\left(\frac{\theta_1^n - \theta_0^n}{z_1 - z_0}\right) - \rho_s C_s K_s\left(\frac{T_0^n - T_1^n}{z_0 - z_{-1}}\right) = 0. \tag{B.2}$$

Atmosphere, transformed coordinate regime:

$$\frac{\theta_j^{n+1} - \theta_j^{n-1}}{2\Delta t} = \left(\frac{L}{z_j}\right)^2\left(\frac{K_{j+1}^n - K_{j-1}^n}{2\Delta\xi}\right)\left(\frac{\theta_{j+1}^n - \theta_{j-1}^n}{2\Delta\xi}\right) + K_j^n\left(\frac{L}{z_j}\right)^2\left(\frac{\theta_{j+1}^n + \theta_{j-1}^n - \theta_j^{n+1} - \theta_j^{n-1}}{(\Delta\xi)^2}\right) - K_j^n\frac{L}{(z_j)^2}\left(\frac{\theta_{j+1}^n - \theta_{j-1}^n}{2\Delta\xi}\right) - \frac{1}{\rho_j C_p}\left(\frac{1000}{p_j}\right)^{0.286}\left(\frac{(F_h)_{j+1}^n - (F_h)_{j-1}^n}{2\Delta\xi}\right)\left(\frac{L}{z_j}\right). \tag{B.3}$$

The first and third terms of the right-hand side of (B.3) cancel below 10 m, as discussed in Appendix A.

Atmosphere, above the transformed coordinate regime:

$$\frac{\theta_j^{n+1}-\theta_j^{n-1}}{2\Delta t}=\left(\frac{K_{j+1}^n-K_{j-1}^n}{2\Delta z}\right)\left(\frac{\theta_{j+1}^n-\theta_{j-1}^n}{2\Delta z}\right)$$
$$+K_j^n\left(\frac{\theta_{j+1}^n+\theta_{j-1}^n-\theta_j^{n+1}-\theta_j^{n-1}}{(\Delta z)^2}\right)$$
$$-\frac{1}{\rho_j C_p}\left(\frac{1000}{p_j}\right)^{0.286}\left(\frac{(F_h)_{j+1}^n-(F_h)_{j-1}^n}{2\Delta z}\right). \tag{B.4}$$

In these equations superscript n denotes time level, and subscript j denotes the vertical grid point. Since in each forecast equation the forecast time level $(n+1)$ appears only at the single grid point j, the system of equations is explicit, and can be solved in a straightforward manner. Using the given radiative parameters, G_r and $F_{h,\,\mathrm{LW}}$, setting $\theta_0 = T_0$ (potential temperature equal to the actual temperature at the ground, $j=0$) and using the atmospheric value of θ_1 and soil value of T_{-1}, we can solve for the interface temperature that satisfies the heat balance equation (B.2). Using this as a boundary condition, (B.1) can be used to forecast the soil temperatures (j negative), and (B.3) and (B.4) to forecast the atmospheric temperatures (j positive).

Appendix C

Numerical stability and consistency

Stability

The Dufort–Frankel scheme described in Appendix B is unconditionally stable for a constant exchange coefficient. When variable exchange coefficient is used, this is no longer guaranteed. From our test calculations, a sufficient condition for stability appeared to be that

$$\frac{\partial K}{\partial z}<\frac{\Delta z}{\Delta t} \quad \text{in (B.3), (B.4).} \tag{C.1}$$

In application, the exchange coefficient profile was examined during each iteration and if this criteria was violated, K was assigned the maximum value which is consistent with (C.1). This is obtained simply by setting

$$K_j = K_{j-1}+\frac{(\Delta z)^2}{\Delta t} \tag{C.2}$$

in such cases. This modification of K was employed only infrequently.

The KEYPS formulation of the exchange coefficient exhibits some sensitivity to the potential temperature gradient at higher elevations. This occasionally results in physically unrealistic variations in the exchange coefficient, which in turn produce oscillations in the temperature profile. To preclude such physically unjustifiable fluctuations of the exchange coefficient, the potential temperature occurring in the KEYPS formulation is smoothed according to

$$\theta_j^n = \frac{\theta_{j+1}^n + 2\theta_j^n + \theta_{j-1}^n}{4}. \tag{C.3}$$

It should be emphasized that this smoothing is applied to the exchange coefficient only, and not to the actual temperature profile.

Consistency

Examination of the truncation error term associated with the Dufort–Frenkel scheme shows that the scheme is consistent to the diffusion process only for sufficiently small ratio of $\Delta t/\Delta z$. Various combinations of time and space steps were tested and the results were compared with exact solutions, until appropriate combinations of Δt and Δz were achieved. A time step of five minutes and the grid spacing indicated in Appendix A were found to be adequate.

(Received 28th October 1974)